PERGAMON

Planetary and Space Science 49 (2001) 345–363

Planetary and Space Science

www.elsevier.nl/locate/planspasci

The plasma wave environment of Europa

W.S. Kurth[a,*], D.A. Gurnett[a], A.M. Persoon[a], A. Roux[b], S.J. Bolton[c], C.J. Alexander[c]

[a] *Department of Physics & Astronomy, The University of Iowa, 613 Van Allen Hall, Iowa City, IA 52242, USA*
[b] *CETP/UVSQ, Velizy, France*
[c] *Jet Propulsion Laboratory, Pasadena, CA 91109, USA*

Received 13 December 1999; received in revised form 30 May 2000; accepted 6 June 2000

Abstract

The Galileo spacecraft has executed nine close flybys of Jupiter's moon Europa for which plasma wave observations were obtained. This paper presents an analysis of the observations from these flybys taking into consideration the variable geometry of the trajectories in an attempt to characterize the general plasma-wave environment associated with the interaction of the Jovian magnetosphere with the moon. A wide variety of plasma-wave phenomena are found to be associated with this interaction. While there are apparently temporal variations which complicate the analysis, a crude model of the distribution of these phenomena around Europa is derived. Primarily on the upstream side of Europa, and working inward to the moon, electron–cyclotron harmonics are first observed, followed by a region within about two Europa radii of the moon with whistler-mode hiss or chorus, and culminating in a region closest to the moon where a band at the upper hybrid resonance frequency is sometimes enhanced over its ambient intensity. The wake region is approximately two Europa radii across and comprises a broadband, highly variable, and bursty electrostatic phenomenon. Upon closer inspection, these bursty emissions appear as solitary structures similar to those in Earth s auroral zone and plasma sheet boundary layer. In addition to the survey of wave phenomena in the vicinity of Europa, we provide density profiles derived primarily from the upper hybrid resonance frequency which is readily apparent throughout most of each of the flybys. Finally, we suggest that the whistler mode, electron cyclotron harmonic, and upper hybrid resonance emissions are driven by some combination of factors including variations in the magnetic field near Europa and the loss and production of plasma at Europa as a result of the interaction of the Jovian magnetosphere with the moon. By analogy with studies of the ion and electron holes and broadband electrostatic noise at Earth and Jupiter, we argue that the electrostatic solitary structures in the wake are associated with currents and beams coupling Europa to Jupiter's ionosphere.

1. Introduction

The first report of plasma waves near Europa was by Gurnett et al. (1998) which included observations from the first two close flybys of that moon by Galileo on the so-called E4 and E6 passes. In this nomenclature, the E indicates that the targeted Galilean satellite flyby for the orbit was Europa and the numeral indicates that the orbit was the 4th (or 6th) of Galileo about Jupiter since its arrival in December 1995. The observations provided by this first report will be discussed in greater detail below. However, the primary features reported by Gurnett et al. for those two flybys include (1) a region of enhanced whistler mode emissions extending over a region slightly more than twice the diameter of Europa, (2) broadband electrostatic emissions over a much narrower region located within the geometric wake, and (3) electrostatic upper hybrid bands which were used (along with the cutoff at the electron plasma frequency) to determine the electron density in the vicinity of Europa. The density measurements showed variable density enhancements relative to the ambient plasma sheet near Europa's orbit (typically 80 cm^{-3}) of 30–80 cm^{-3}. Gurnett et al. argued that the plasma waves were probably generated by loss cone distributions of energetic electrons. These loss cones are likely due to the loss of electrons to Europa. They also argued that enhanced electron densities and reduced magnetic field strengths (reported by Kivelson et al. (1997) for the E4 pass) could decrease the cyclotron resonance energy, hence increase the whistler mode growth rate in the vicinity of Europa.

Since the Gurnett et al. (1998) report, Galileo has also executed close flybys of Europa on the E11, E12, E14, E15, E17, E19, and E26 passes for which the plasma-wave instrument obtained useful observations. Most of these passes are part of the Galileo Europa Mission, an extension of the prime mission which had as one of its prime objectives intensive studies of Europa and its magnetospheric

* Corresponding author. Tel.: +001-319-335-1926; fax: +001-319-335-1753.
E-mail address: william-kurth@uiowa.edu (W.S. Kurth).

0032-0633/01/$ - see front matter
PII: S0032-0633(00)00156-2

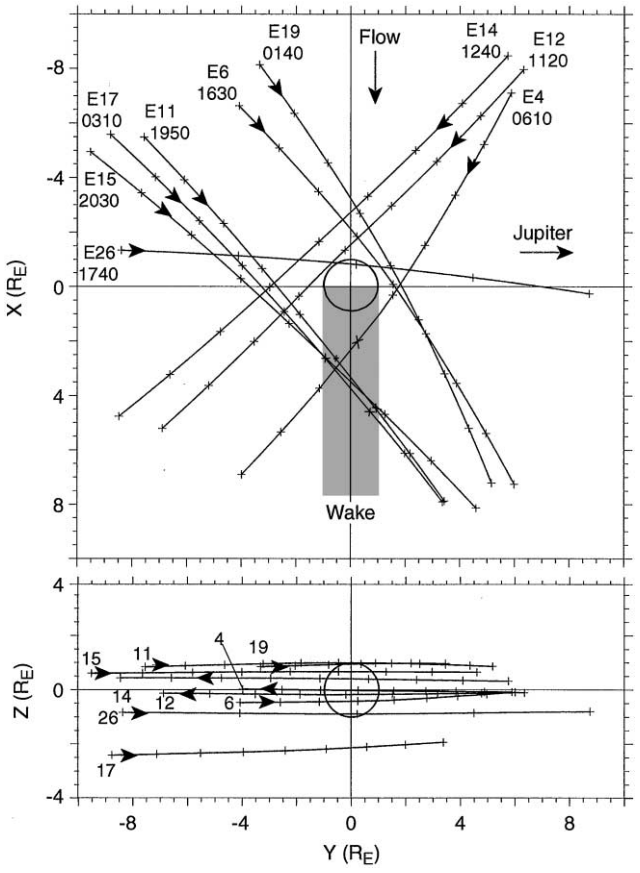

Fig. 1. The geometry of the nine Galileo flybys of Europa for which plasma-wave observations were obtained. The upper panel shows the projection of the trajectories into the plane defined by the nominal corotational flow direction (x) and the direction to Jupiter (y). The bottom panel shows the trajectories projected into the z–y plane where the z direction is parallel to Jupiter's rotation axis.

environment. Fields and particles data were not returned during the E13 pass because of data rate limitations near solar conjunction. Observations from the E16 and E18 passes were lost due to radiation-associated anomalies on the spacecraft.

The comprehensive set of observations now in hand provides measurements at a wide variety of geometries with respect to Europa. In this paper we will present the complete set of observations and attempt to show that the plasma wave features are organized to some extent by their location with respect to Europa and its plasma wake. However, we will also show that there remain some variations which cannot necessarily be explained by a simple map. We will also briefly discuss the possible origins of the wave phenomena observed.

Fig. 1 shows the geometry for each flyby for which we have observations. The coordinate system used is fixed at Europa's center with the x-axis in the nominal corotational flow direction, the z-axis parallel to Jupiter's rotational axis, and the y-axis toward Jupiter. The upper panel shows the trajectories projected onto the x–y plane. The direction of motion is in all cases towards positive x or from top to bottom in this display. Each trajectory is labeled with the starting time of the portion of the trajectory shown in spacecraft event time (SCET). Tick marks are at 10-min intervals from this starting time. The bottom panel of Fig. 1 shows the trajectories in the y–z plane such that the reader is viewing Europa from a position in the geometric wake. The various trajectories are only marked with the orbit number; arrows indicate the direction of motion. Notice that there is reasonable coverage of the region close to Europa including upstream and wake passes as well as passes on both the Jupiter-facing and anti-Jupiter hemispheres of Europa. Importantly, there is generally more than one pass sampling similar positions in this coordinate system which is essential to our understanding of general trends in the occurrence of plasma wave features described below. Notice that most of the passes are reasonably close to Europa's equator. Exceptions are E17, which is approximately 2 Europa radii (R_E) south of the moon's equator, and E11 and E19 which are both approximately 1 Europa radius north of the equator. E26 is a potential southern flux tube crossing.

Table 1 provides a summary of some important flyby geometry parameters. Each flyby is labeled with its designator in column 1. Column 2 gives the date and time of closest approach. The third column provides the altitude of the spacecraft at closest approach and the fourth column characterizes each flyby as either wake or upstream. If the projection of the trajectory into the x–y plane crosses the positive x-axis, it is called a wake passage, otherwise it is labeled "upstream". Also, throughout this paper, our reference to the geometric wake is to the volume of space with $|y| \leqslant 1R_E$. The fifth column gives the magnetic latitude λ_m (with respect to Jupiter) of Galileo at the time of the encounter; Kivelson et al. (1999) suggest that Europa's position with respect to the plasma disk may be important in determining the nature of its interaction with the Jovian magnetosphere and the magnetic latitude provides a first-order measure of this factor. Column 6 is the system III longitude λ_{III} of Galileo at the time of closest approach. Column 7 is the local time of Galileo with respect to Jupiter while column 8 indicates whether the flyby is primarily on the day- or night-side of Europa. Finally, the last column characterizes each flyby as to whether it passes over the Jupiter-facing or anti-Jupiter hemisphere of Europa, based on whether the projection of the trajectory into the x–y plane crosses the positive or negative y-axis, respectively.

The observations presented herein are from the Galileo plasma wave instrument which is described thoroughly in Gurnett et al. (1992). The instrument measures the electric field component of waves in the frequency range of 5.62 Hz–5.6 MHz using a single-axis dipole antenna with an effective length of 6.6 m and magnetic fields in the frequency range of 5.62 Hz–160 kHz with a pair of magnetic search coils. The high-frequency search coil is used

Table 1
Galileo Europa flyby geometries

Flyby	Time of closest approach	Alt. (km)	Upstream/ wake	Magnetic latitude (○)	λ_{III}(○)	LT[a] (h)	Day/night	Jupiter/Anti-jupiter hemisphere
E4	Dec. 19, 1996 0652 : 58	692	Wake	6.6	157	16.7	Night	Jupiter
E6	Feb. 20, 1997 1706 : 10	586	Upstream	−7.6	340	12.9	Night	Jupiter
E11	Nov. 6, 1997 2031 : 44	2043	Wake	8.7	223	11.0	Day	Anti-Jupiter
E12	Dec. 16, 1997 1203 : 20	201	Upstream	0.9	118	14.7	Day	Anti-Jupiter
E14	Mar. 29, 1998 1321 : 05	1644	Upstream	9.1	184	14.4	Day	Anti-Jupiter
E15	May 31, 1998 2112 : 57	2515	Wake	−0.5	293	10.1	Day	Anti-Jupiter
E17	Sep. 26, 1998 0354 : 20	3582	Wake	3.6	138	9.9	Day	Anti-Jupiter
E19	Feb. 1, 1999 0219 : 50	1439	Upstream	5.6	256	9.8	Night	Jupiter
E26	Jan. 3, 2000 1759 : 43	198	Flux tube	−9.6	2	2.9	Night	Jupiter

[a]Local time with respect to Jupiter.

for frequencies above 2.4 kHz. The low-frequency search coil is tuned for frequencies below 2.4 kHz. A failure in the low-frequency search coil or its signal path on 14 September 1997 during the tenth orbit resulted in increased levels of noise and a serious reduction in sensitivity for frequencies below 2.4 kHz. Hence, low-frequency magnetic field measurements for the E11 flyby and later are not very useful. However, in some cases, intense electromagnetic signals can be seen and this is sufficient to justify the identification of some waves as being electromagnetic as opposed to electrostatic. The lack of magnetic signatures in this frequency range, however, do not justify the identification of electrostatic modes.

The primary measurements are made using a multichannel analyzer, a medium frequency receiver, and a high-frequency receiver to provide a single 152-channel spectrum over the entire frequency range once every 18.67 s. For the Europa observations, the multichannel analyzer and medium frequency receiver toggle between the electric antenna and the search coils every 18.67 s. Therefore, the overall temporal resolution below 100 kHz is 37.33 s for both electric field measurements and magnetic field measurements. Above 100 kHz an electric field spectrum is acquired every 18.67 s. Wideband waveform measurements are also obtained during all but the E17 flyby. These measurements utilize one of three broadband channels of 1, 10, or 80 kHz bandwidth coupled with an automatic gain control amplifier to produce series of 4-bit digital waveforms. The sample rate for the three analysis bandwidths are 3200, 25, 200, and 201,600 samples per second, respectively. For all of the Europa wideband measurements, the waveform series were obtained with the electric antenna and consist of 864 consecutive measurements occurring once every $n \cdot 1.33$ s, where n is 1, 2, or 4. The results are measurements with high spectral resolution but with resolution between spectra which is considerably poorer than is usually the case with wideband measurements. This poor temporal resolution is a direct result of the loss of high telemetry rates due to the failure of the high gain antenna on Galileo.

2. Observations

A remarkable aspect of the set of nine Europa flybys reported herein is the variety of signatures seen from one encounter to the next in the plasma-wave spectrum. Figs. 2–4 provide an overview of the measurements and a brief survey of these will convince the reader of this variety. A primary goal of this paper is to provide some order to this apparently disordered situation; we will attempt to show that there are common features observed in some regions of this interaction.

The format of these figures is similar so as to aid the reader in comparing them. The upper panel of each figure provides the intensity of the magnetic field component of waves as a function of frequency and time in the frequency range of 5.6 Hz–100 kHz. The lower panel provides the same type of information for the electric component of the waves, but to a maximum frequency of 5.6 MHz. For both panels, the intensity of the waves is represented as dB above background according to the color bar on the right. A total dynamic range of 72 dB is used for this entire set of figures. We have used the measured magnetic field intensity provided by the magnetometer team (Kivelson et al., 1992; M. Kivelson, pers. commun., 1999) to determine the electron–cyclotron frequency $f_{ce} = 28 \cdot |\mathbf{B}|$ where f_{ce} is in Hz and $|\mathbf{B}|$ is in nT. Contours of f_{ce} are indicated on each panel in Figs. 2 and 3 except for the E6 pass (Fig. 2b) for which no magnetic field measurements are available. Magnetic field measurements are also not yet available for the E26 pass. We note the radial distance to Europa across the abscissa. Also included is the magnetic latitude λ_m with respect to Jupiter. The latter is important since some plasma-wave features are common near $\lambda_m = 0$, particularly the electron–cyclotron harmonic emissions (Kurth et al., 1980) and to a lesser extent whistler-mode chorus. This must be considered when determining whether or not a particular feature is associated with Europa or simply the ambient magnetosphere.

For all passes except E17 the full resolution recorded data are used for these illustrations. For E17, no recorded data are available and the so-called real-time science data

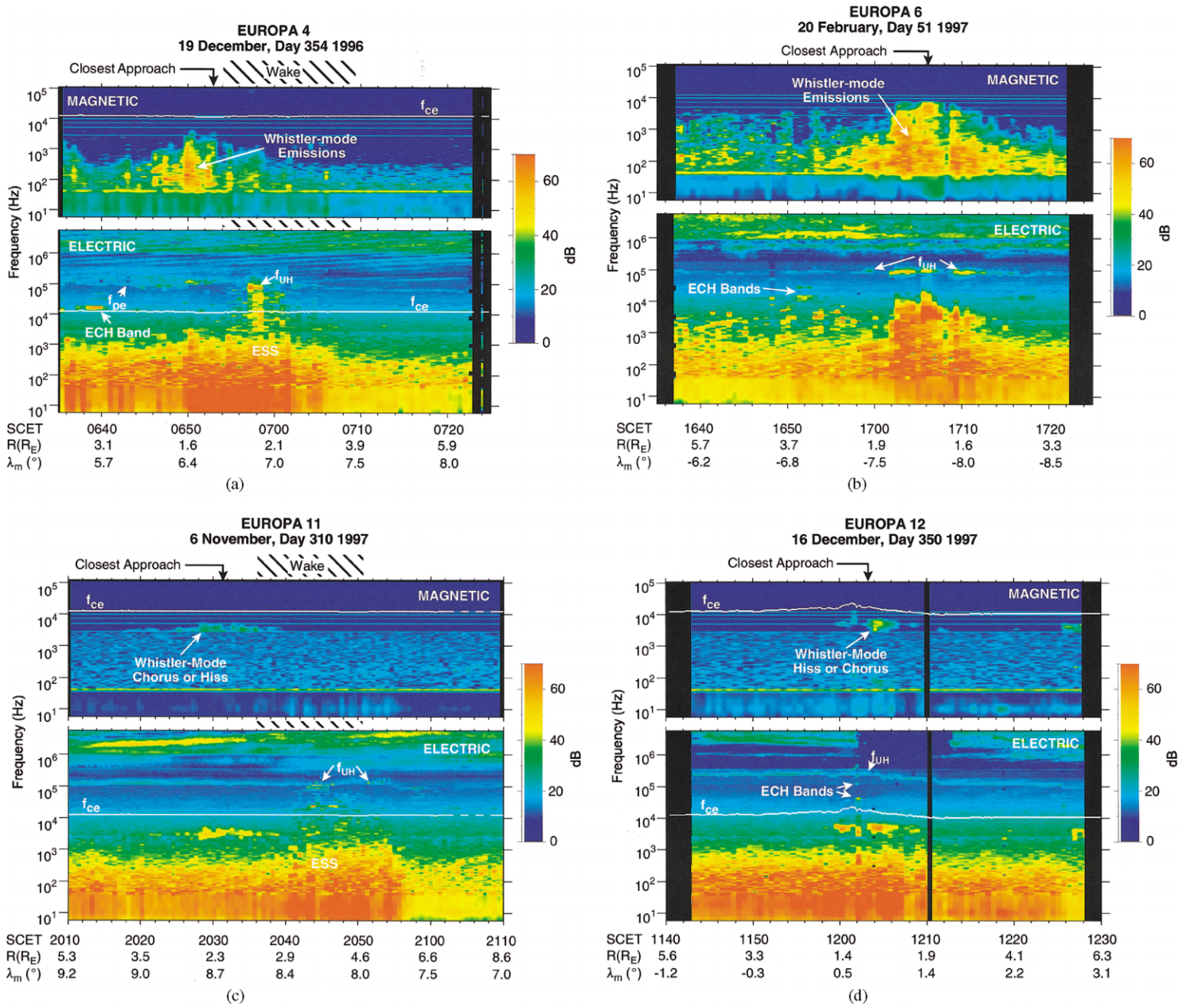

Fig. 2. Frequency-time spectrograms providing the sweep-frequency receiver observations for the (a) E4. (b) E6, (c) E11, and (d) E12 flybys. The upper panel of each shows the magnetic field component of waves as a function of frequency and time. The lower panels provide the intensity of the electric component of the waves. The white line in all but the E6 data is the electron–cyclotron frequency based on the measured magnetic field provided by M.G. Kivelson (pers. commun., 1999).

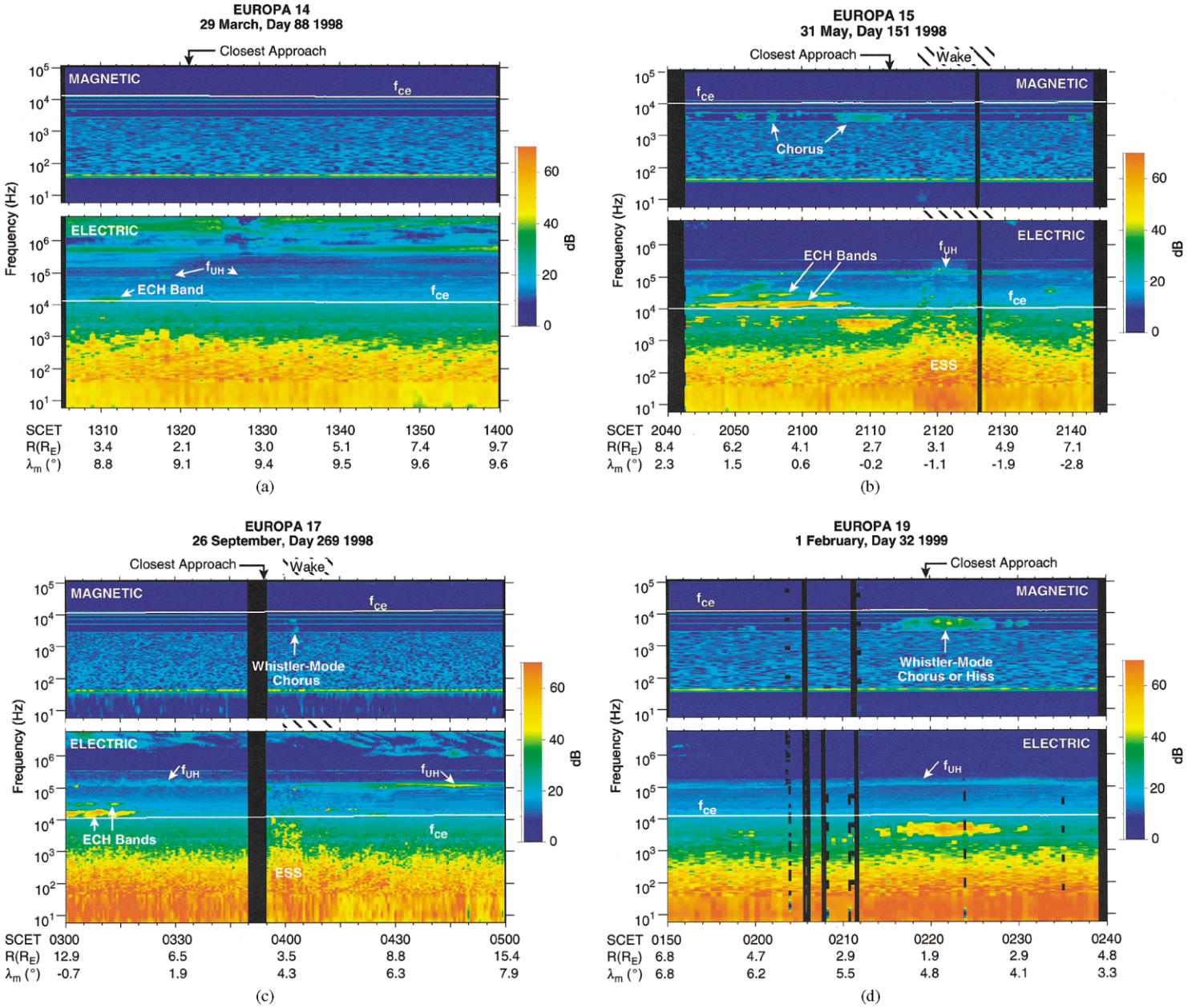

Fig. 3. Same as Fig. 2 for the (a) E14, (b) E15, (c) E17 and (d) E19 encounters.

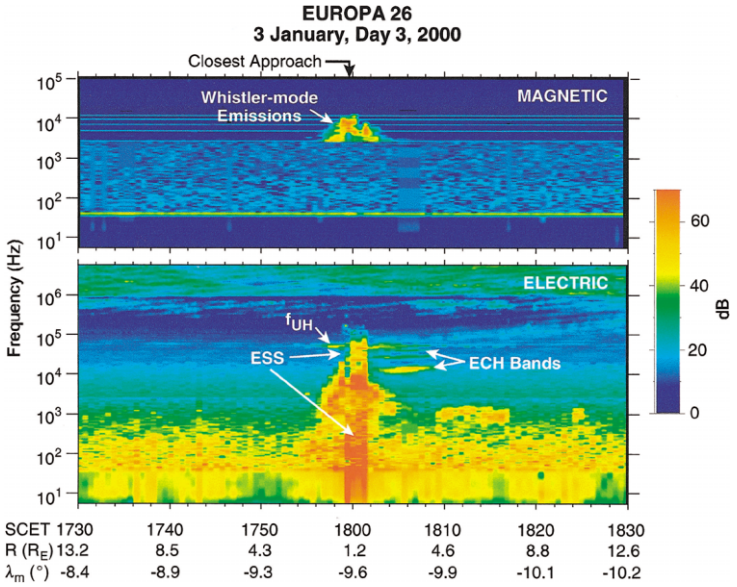

Fig. 4. Same as Figs. 2 and 3 for the E26 encounter.

are used which incorporate a lossy integer cosine transform compression scheme with a compression ratio of about 5 : 1. In this scheme, the basic frequency and time resolution is maintained at the expense of amplitude accuracy. We believe the uncertainty in amplitude is typically a few dB for the most extreme compression ratios (13 : 1). The fact that compression artifacts such as "tiling" effects are not readily apparent in the E17 data suggests that the amplitude uncertainty is considerably less than this. Finally, it should be noted that we have included the data from the low-frequency (< 2.4 kHz) search coil for passes from E11 and beyond even though the sensitivity is very poor. This is done primarily to keep the format of the presentations the same; in a few cases there are some magnetic signatures which can be seen even with the reduced sensitivity.

2.1. E4 Observations

The plasma-wave observations from the E4 pass shown in Fig. 2a have been described by Gurnett et al. (1998), but we shall summarize them here for ease in comparing with the later, heretofore unpublished observations. As seen in Fig. 1, this is a wake pass for which closest approach occurs near the edge of the geometric wake on the Jupiter-facing side of Europa. The most obvious feature in the magnetic spectrogram in Fig. 2a is the rather broadband noise below about 5 kHz (below about one-half the electron–cyclotron frequency). This emission occurs at and just prior to closest approach; it is significantly weaker within the wake region. Given that these waves are below both the electron–cyclotron and plasma frequencies (see below) these waves are propagating in the whistler mode and are almost certainly analogous to what is referred to as whistler-mode hiss in the terrestrial magnetosphere. Between 0649 and 0653 SCET the measured ratio of cB/E of ~ 60 is very close to the index of refraction for the electron–cyclotron frequency of about 12 kHz and electron-plasma frequency of about 100 kHz as would be expected for whistler-mode waves.

The electric field spectrogram in Fig. 2a shows a number of features. First, there is an electrostatic electron–cyclotron harmonic (ECH) band near 0640 SCET just above f_{ce}. Such a band is sometimes also referred to as a $3f_{ce}/2$ band since it lies between the fundamental and second harmonic of f_{ce}. Such emissions are not uncommon in the inner Jovian magnetosphere, but usually only intensify within about a degree of the magnetic equator (Kurth et al., 1980). Since the Jovian magnetic latitude at 0640 is about 5.7°, it is likely that this feature is associated with the magnetosphere–Europa interaction and not simply a feature of the ambient magnetosphere. There is a general enhancement in the electric field spectrum below about 3 kHz, especially between about 0650 and 0706 SCET. It is somewhat surprising that this enhancement does not coincide well with the enhanced whistler-mode emissions seen in the upper panel and suggests that the waves after about 0654 are primarily electrostatic. The cB/E ratio at 300 Hz in the time frame of 0656–0705 is of order 3, significantly lower than for the earlier period with strong magnetic fields. The electrostatic emissions extend well above f_{ce} to f_{UH} in this time period suggesting the term broadband electrostatic noise (Gurnett et al., 1976; Gurnett and Frank, 1977; Barbosa et al., 1981). Here f_{UH} is the upper hybrid resonance frequency given by $f_{UH}^2 = f_{ce}^2 + f_{pe}^2$. Based on an analysis of the wideband waveform measurements below, we identify the broadband electrostatic feature as electrostatic solitary structures (ESS). We investigate the nature of these emissions in detail in Section 3.1. At higher frequencies, there is an intensification near 0658 labeled f_{UH} in Fig. 2a which Gurnett et al. identified as the upper hybrid

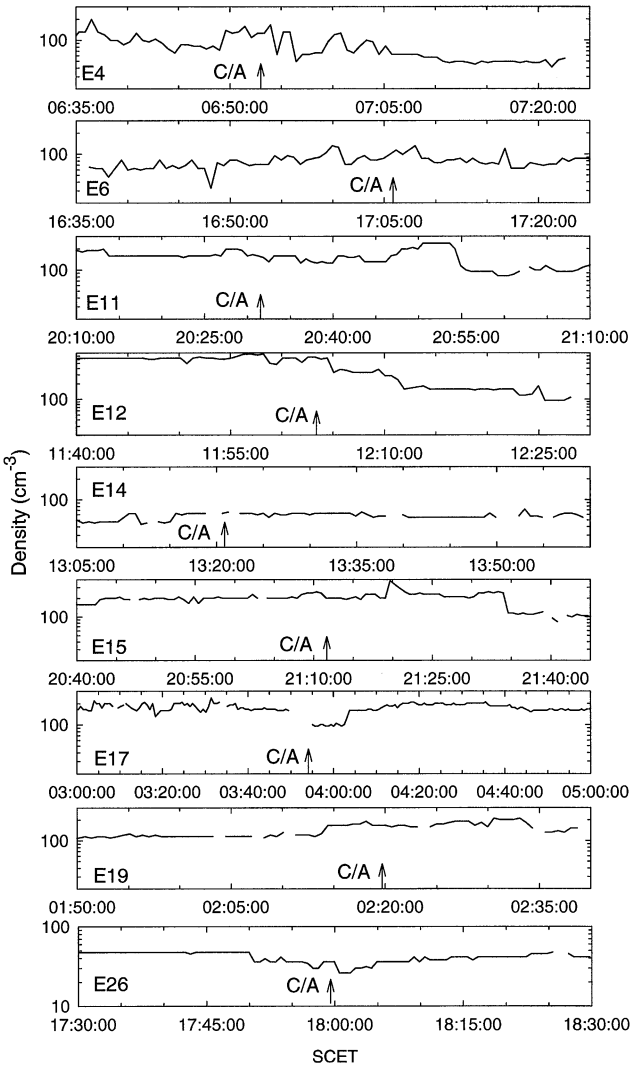

Fig. 5. Electron-density profiles based on the upper hybrid resonance band observed during each of the Europa flybys.

resonance band. Prior to this time, but at about the same frequency, near 100 kHz, radio emissions can be seen to cut off quite sharply, suggesting that this is the electron plasma frequency. Actually, this cutoff could occur remotely from the spacecraft, so this is, strictly speaking, an upper limit to the local electron density. The intense narrowband upper hybrid bands, however, should provide a good local measurement of the electron density. Note that since $f_{UH} \gg f_{ce}$, $f_{UH} \simeq f_{pe}$. Gurnett et al. show an electron density profile based on the cutoff at f_{pe} and the f_{UH} bands and show that there are perturbations of the ambient electron density of about 30–80 cm^{-3}. The density profile is reproduced in the top panel of Fig. 5, along with those from the other flybys presented herein. Finally, at frequencies above f_{pe} and f_{UH}, Jovian hectometric radiation is seen throughout the interval.

Wideband data were obtained during the E4 flyby in the 80-kHz mode with one 864-point series obtained every 2.67 s. Given the sample rate of 201,600 s^{-1}, a waveform series requires about 4.3 ms to collect, hence, the duty cycle is very small, about 0.2%. Nevertheless, reasonable frequency-time spectrograms can be obtained with these data as shown in Fig. 6. However, this mode will not be particularly useful for identifying the full temporal evolution of phenomena in the range of a few ms–1 s. Hence, features like chorus will be difficult to identify. The spectrograms do provide high spectral resolution measurements and measurements of the evolution of spectra over time scales of seconds to minutes. Fig. 6 shows both the ECH and upper hybrid bands mentioned above in very high resolution. These phenomena often do not show significant temporal structure, hence, the low duty cycle does not likely hamper these measurements. The low-frequency electric field component of the whistler-mode emissions are seen at the bottom of the spectrogram, particularly near 0650, but the 4.3 ms sample length provides only about 230 Hz resolution, hence, these emissions are not very prominent. One other feature of note is the very broadband response between about 0655 and 0703 SCET, generally within the early portion of the wake passage. It is clear that these broadband features are very brief, apparently changing character on time scales of individual spectra, or about 2.67 s.

We have examined the broadband bursty signatures observed in both Figs. 2a and 5 in greater detail in Fig. 7. This figure shows the raw waveforms from two intervals within the wake. Plotted is the potential between the electric antenna inputs as a function of time. The top panel begins at 0658:19.947 SCET and shows a very confusing set of waveforms. There is a brief period of apparently sinusoidal oscillation at high frequency centered near the 1.7-ms point in the waveform; these are evidently waveforms associated with the upper hybrid emissions near 70 kHz. The dominant feature, however, is a series of relatively large amplitude solitary structures, very similar to the electrostatic solitary waves shown to underlie the broadband electrostatic noise in the terrestrial magnetosphere (Matsumoto et al., 1994). The low-frequency variation provides a poor background upon which to observe some of the solitary waves, but the example near 2.9 ms shows the characteristic bipolar form quite well. The bottom panel is from 0702:19.947 near the end of the interval of broadband noise and shows an excellent example of an isolated solitary structure. The duration of the solitary structures in this illustration are of order 0.1 ms, corresponding to a fundamental frequency of about 10 kHz. They also consistently show first a negative, then a positive variation in the voltage. However, without knowing the direction of motion, the polarity of the structures cannot be unambiguously determined. The interpretation of these structures and their significance are discussed in Section 3.1.

2.2. E6 Observations

As seen in Fig. 1, the E6 flyby passes on the upstream side of Europa and has a closest approach altitude of 586 km

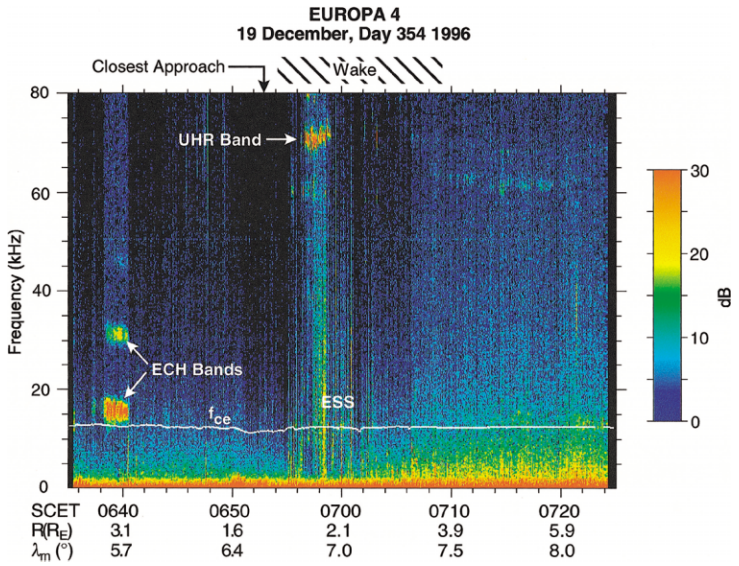

Fig. 6. Electric field wideband spectrogram for the E4 flyby in the 80-kHz mode.

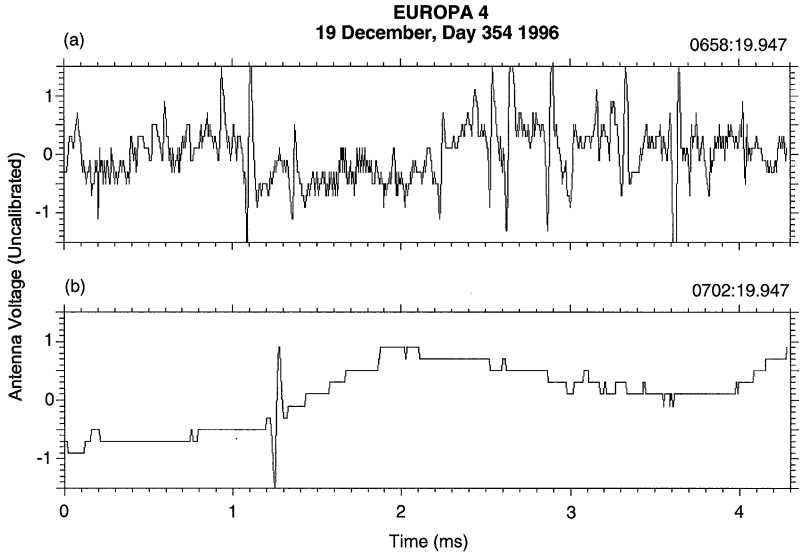

Fig. 7. Waveforms from E4. Plotted is the antenna potential difference, proportional to the electric field, as a function of time for two intervals in the E4 wake.

at 1706:10 over the Jupiter-facing hemisphere. Fig. 2b shows the wave observations from this flyby, which were also discussed by Gurnett et al. (1998). Unlike the situation for E4, the most intense signatures in both the electric field and magnetic-field spectrograms occur more-or-less simultaneously and almost certainly are whistler-mode emissions. The magnetometer did not provide measurements during this pass, but given an electron–cyclotron frequency of about 12 kHz, similar to that observed during the E4 pass, these emissions are confined to the frequency regime below f_{ce}. The cB/E ratio at 1704 SCET at 300 Hz is 73, hence, consistent with the whistler mode (Gurnett et al., 1998). The electric-field component extends to somewhat higher frequencies than the magnetic-field component, therefore, it is possible that this high-frequency extension, at about 15 kHz, is the first electron–cyclotron harmonic band just above f_{ce}. Another occurrence of electron–cyclotron harmonic emissions is seen at about 15 kHz near 1652 SCET. The upper hybrid band is intensified near closest approach and extends weakly over the remainder of the spectrogram in Fig. 2b. Gurnett et al. (1998) have derived a density profile based on the frequency of the upper hybrid band. This is reproduced in the second panel in Fig. 5. Unlike E4, there is no evidence for broadband electrostatic waves during this pass.

Wideband observations for the E6 flyby are presented in Fig. 8. The instrument mode was the same as that

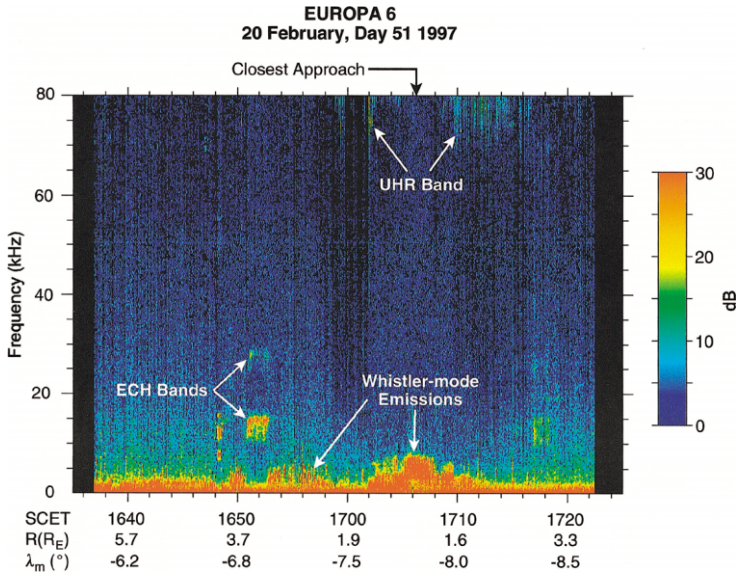

Fig. 8. Wideband spectrogram for the E6 flyby in the 80-kHz mode.

for E4, covering the frequency range up to 80 kHz. The whistler-mode emissions are prominent below 10 kHz centered on closest approach. Other whistler-mode emissions are seen centered at about 1655 SCET with a somewhat lower maximum frequency. These earlier emissions appear to be more bursty in time than those at closest approach. It is possible that the temporal structure here implies chorus emissions, but as explained above, the relatively poor temporal resolution (2.67 s between spectra in this case) makes it difficult to identify chorus elements with similar temporal duration. The electron–cyclotron harmonic emissions near 1652 SCET are much more prominent in this display than in the sweep frequency data shown in Fig. 2b. This is due, in part, to the linear frequency axis in Fig. 8. Evidence for the upper hybrid band is visible at the high-frequency edge of the spectrogram. Again, there is no evidence for broadband electrostatic waves in this spectrogram.

2.3. E11 Observations

Fig. 1 shows that the E11 pass approaches from the anti-Jupiter direction and passes through the geometric wake after closest approach which occurs at 2031:44 SCET on 6 November, 1997. The closest approach altitude is 2043 km. Fig. 2c provides an overview of the E11 observations. The strong, broadband whistler-mode emissions are not present in this flyby, unlike both of the previous passes. Recall that the low-frequency search coil or electronics associated with its signal failed on the previous orbit, so it is somewhat problematic to observe such emissions. It should be pointed out, however, that there is a response below about 40 Hz between about 2035 and 2056 SCET which we believe to be a reliable detection of wave magnetic fields albeit with a strong attenuation factor. A feature is observed by the high-frequency search coil with a bandwidth of about 2 kHz, centered near closest approach. A similar feature in the electric spectrogram confirms the emission is of relatively small bandwidth. Based on these observations, it would be reasonable to suggest that this feature is chorus. Wideband observations discussed below bear on this identification, however. Broadband electrostatic waves of a very bursty nature exist between about 2040 and 2049 SCET above f_{ce}. This feature could extend to as late as 2056 SCET at frequencies below f_{ce}, but without reliable magnetic field measurements between 40 Hz and 2.4 kHz, we cannot rule out whistler-mode emissions as the mode. The higher frequency broadband waves fall within the geometric wake, but appear to be limited to a smaller interval than the wake. If the lower frequency waves extending to 2056 SCET are electrostatic in part, this wave feature extends across a region in space similar in size to the geometric wake, but displaced towards Jupiter by a few minutes. The offset to later times suggests that the flow imposed by the magnetospheric plasma has an inward radial component. The upper hybrid band for this pass shows a modest increase in frequency centered around 2050 SCET with a peak of about 150 kHz corresponding to a maximum density of about 275 cm^{-3}. This density peak is situated in the wake and is certainly suggestive of a source of plasma at Europa that is scavenged by the interaction of the Jovian magnetosphere as it sweeps past the moon. The UHR band extends earlier but fades away by about 2100 after the flyby. The earlier portion of the band has a somewhat extended bandwidth with a smooth temporal variation. These characteristics are those of a band of radio emissions with a lower cutoff at the plasma frequency. The density profile determined from these features is given in Fig. 5.

Fig. 9 shows the wideband observations obtained in the 10-kHz mode during the E11 flyby. The band-limited

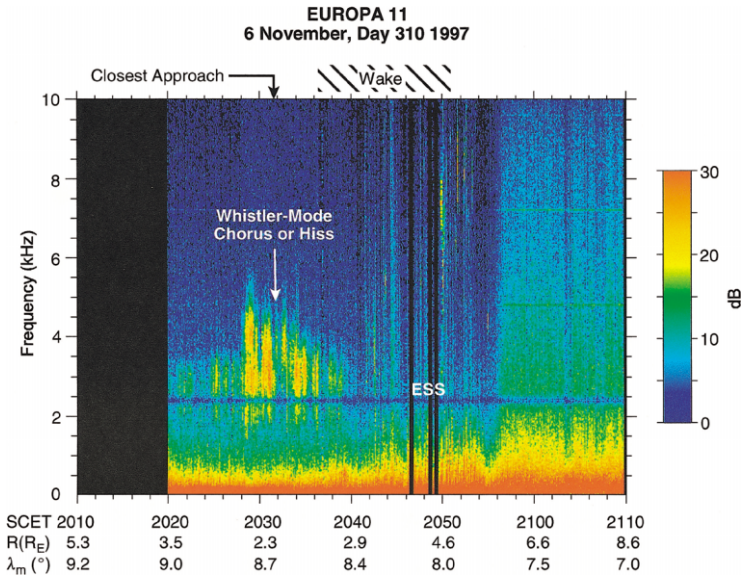

Fig. 9. Wideband spectrogram for the E11 flyby in the 10-kHz mode.

whistler-mode emission dominates the spectrogram near closest approach. It is not clear that these observations settle the question as to whether these are hiss or chorus emissions. There is a fair amount of temporal structure in this feature, but again, the temporal resolution of 1.33 s does not allow for the identification of chorus elements. Furthermore, variations in the automatic gain control from other in-band signals, perhaps at lower frequencies, may masquerade as amplitude variations in this particular feature. The interval from about 2042 to 2054 SCET is characterized by broadband emissions with a rapidly varying character, very similar to the broadband electrostatic emissions shown in the E4 wake in Fig. 6. An examination of the waveforms for these data show similar solitary structures to those shown in Fig. 7 with dramatic differences in character from one waveform series to the next. The apparent broadband intensification seen in Fig. 9 after about 2056 SCET is an artifact of the automatic gain control circuitry and simply represents an increase in gain as the spectral density in the 10-kHz band decreases during this time period as confirmed by the data in Fig. 2c. The appearance of the second and third harmonic of the 2.4-kHz power supply frequency in this interval is further evidence of an increase in receiver gain.

2.4. E12 Observations

The E12 flyby is an upstream pass with one of the smallest closest approach altitudes of all of the Europa flybys at 201 km; the E26 pass has a closest approach altitude of 198 km. The closest approach occurs at 1203:20 on 16 December, 1997 over the anti-Jupiter hemisphere of the moon as shown in Fig. 1. The overview of the wave observations for this flyby are given in Fig. 2d. There is low-frequency (< 1 kHz) electromagnetic noise virtually throughout this pass which is almost featureless except for a diminution at 1208 SCET and another decrease in amplitude near the end of the plot at 1226 SCET. The magnetic field measurements are hampered at low frequencies as they were in E11, but there is a significant magnetic signal which appears below 40 Hz for virtually the entire plotted interval. Whistler-mode hiss or chorus appears nearly centered on closest approach, generally below about one-half of the electron–cyclotron frequency. At 1202 SCET, just prior to closest approach, there appears to be a very brief instance of electron–cyclotron harmonic emissions, most prominent just above f_{ce} where one would expect the $3f_{ce}/2$ band. An additional harmonic appears much more weakly near 100 kHz. This flyby occurs very close to the Jovian magnetic equator, hence, it is not possible to uniquely identify the whistler mode emissions near $f_{ce}/2$ or the ECH bands as being tied to the presence of Europa as both of these types of emissions are commonly seen at the magnetic equator (Kurth et al., 1980), especially the ECH bands.

The band at the upper hybrid resonance frequency is clearly seen throughout this interval, however, it shows no intensification near the Europa closest approach as it did on the previous passes. It is interesting that the frequency of the band is continuously decreasing throughout the interval; Galileo is outbound during this flyby, but it is not clear that this decrease in density is necessarily simply a radial distance effect. A latitude effect is also possible. Based on the frequency of the band, the density at 1143 SCET is $\sim$ 600 cm^{-3} and drops to about 100 cm^{-3} at 1228 SCET. The density profile is shown in the fourth panel of Fig. 5. We note the abrupt dropout in the hectometric signal at 1202 SCET and the signal's reappearance at about 1213 SCET. This is an occultation of the hectometric radio source (located near

Jupiter on auroral field lines) by Europa. Kurth et al. (1997) used a similar occultation by Ganymede to determine the source location of the hectometric radiation. Similar analyses have begun for this occultation, but the occultation analysis is not central to the physics of the magnetosphere–Europa interaction, hence, will not be discussed here further.

Wideband measurements in the 1-kHz mode were obtained during this flyby, however, as suggested by the nearly featureless spectrum below 1 kHz in Fig. 2d, the wideband spectrogram provides little more information than the observations in Fig. 2d.

2.5. E14 Observations

The E14 flyby geometry is similar in many respects to that of E12 as can be seen in Fig. 1. The primary difference is that the closest approach altitude is 1644 km, eight times higher than that of E12. The observations presented in Fig. 3a are remarkable in that they show virtually no signature of the flyby at all. There is a very weak upper hybrid band observed intermittently throughout the plotted interval near 70 kHz, however, the band has all but faded out near closest approach at 1321:05 SCET. Densities determined from this band are given in Fig. 5. Based on the electric field spectrogram, there is a broadband signal below 1 kHz, but this is significantly weaker than similar features at the other flybys and could reasonably be associated with the ambient Jovian magnetosphere at this radial distance. There is a very weak band just above f_{ce} at about 1311 SCET which is likely an ECH band. This is high enough in magnetic latitude that it is not likely associated with the ambient magnetosphere. However, this is probably the only feature related to Europa in this flyby. It is most likely that this flyby, being significantly distant and upstream, simply does not enter a region where Europa-specific instabilities have had a chance to grow to significant amplitudes.

2.6. E15 Observations

As seen in Fig. 1, the geometry of the E15 flyby is quite similar to that of E11, including a wake passage and closest approach (2515 km) on the anti-Jupiter hemisphere of the moon at 2112:57 SCET. Fig. 3b shows that this is one of the more complex data sets of the Europa collection. Since the Jovian magnetic equator crossing occurs at 2107:30 SCET, it is almost certain that some of these waves are associated with the ambient magnetosphere at the magnetic equator and not Europa. For example, the ECH bands here seen centered on about 2055 SCET all lie within about 1.9° of the magnetic equator, hence, would be expected in the ambient magnetosphere (Kurth et al., 1980); we conclude that these are not likely associated with Europa, but there is no clear way to eliminate this possibility. Similarly, we expect that the chorus emissions falling between about 2043 and 2115 SCET are those expected in the equatorial magnetosphere; there is no way to rule out an association with Europa, however. There is some evidence for the low-frequency, broadband whistler-mode emissions below several hundred Hz beginning at about 2116 and continuing beyond 2130 SCET, even though there is little or no signature in the wave magnetic field data. Bursty electrostatic emissions are visible within at least the earlier portion of the wake passage as indicated in Fig. 3b, especially between 2116 and 2119 SCET. There is evidence for a high harmonic ECH band just below f_{UH} during this interval. Throughout the plotted time period up to about 2135 SCET the upper hybrid band is fairly constant in frequency near 125 kHz, consistent with a density of about 200 cm^{-3} (see the density profile in Fig. 5). There is some additional structure and enhancement in this band between about 2119 and 2125 SCET which may differentiate between the ambient UHR band and that of Europa's wake. A peak in the electron density near 2120 SCET reaches nearly 400 cm^{-3}.

Fig. 10 shows the rather spectacular wideband observations in the 10 kHz mode obtained during this flyby. The highly-structured emissions below about 6 kHz exhibit a gap at one-half the electron–cyclotron frequency and, for this reason, appear very similar to the chorus emissions observed by Voyager and described in detail by Coroniti et al. (1984). Because of the 1.33-s temporal resolution of these wideband measurements, it is difficult to see the actual chorus elements, but some hint that the discrete elements exist can be seen in the band above the gap between 2048 and 2100 SCET. It is the similarity of these observations to those studied by Coroniti et al. which leads us to identify these and the later emissions (centered near 2110 SCET) as chorus emissions. Emissions with a similar spectrum are observed briefly centered at 2130 SCET, and we identify these as chorus emissions, as well.

In the period of 2116 to about 2125 SCET bursty, broadband emissions are observed similar to those seen in other wake regions, for example those from the E4 pass. Fig. 11 shows a series of waveform observations obtained between 2123:49 and about 2124 SCET with a sample rate of 25,200 s^{-1}. The upper 5 panels show consecutively-acquired waveform series with a spacing of 1.33 s, the highest resolution available in this telemetry mode. The bottom panel is taken 4 s after this sequence. The most remarkable aspect of these observations is the dramatic changes not only from one waveform series to the next, but also the abrupt changes occurring within some of the series, for example in the top three panels. In panel (a) there is a brief burst of high-frequency emissions centered on 20 ms and lasting for about 5 ms. These are more-or-less sinusoidal waves with a frequency of several kHz. At about 28 ms into panel (b) a large-amplitude, low frequency emission begins and has a frequency of several hundred Hz. The waveform deviates significantly from a sinusoid, however, and we suspect that this could be a train of large amplitude electrostatic solitary structures with relatively long time scales. Panel (c) exhibits the rather abrupt onset of a

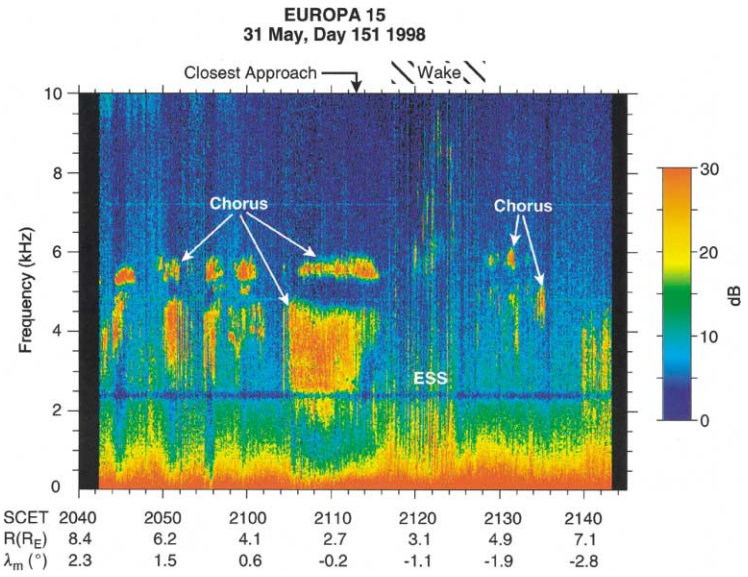

Fig. 10. Wideband spectrogram for the E15 flyby in the 10-kHz mode.

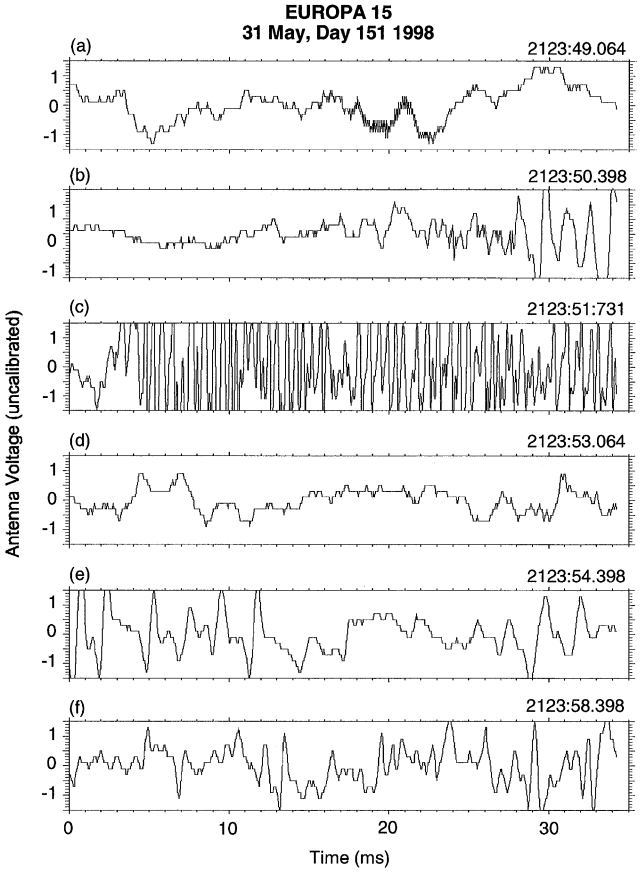

Fig. 11. A series of waveforms from the E15 flyby showing the tremendous variations over time scales of seconds or less in the nature of the waves found in the wake region.

quasi-sinusoidal emission beginning at about 3 ms into the panel and with a characteristic frequency of about 2 kHz. Again, toward the end of this panel the waveforms are distinctly not sinusoidal and we again attribute this character to a train of electrostatic solitary structures as opposed to an extended wave packet. Panel (d) represents what might be considered the quiet background waveform with relatively low-frequency variations with no clear sinusoidal variations. The short antennas on Galileo are subject to shot-noise and this waveform may simply be characteristic of this phenomenon. Panels (e) and (f) in Fig. 11 show a series of waveforms which at times appear to be sinusoidal over a few cycles and at other times appear to be solitary, such as some of those seen in Fig. 7. The wake region of the E15 pass, then, is characterized by a rapidly varying set of waves and solitary structures with highly variable characteristic frequencies. Unlike the solitary waves in Fig. 7, those in Fig. 11 have durations of from 1 to 3 ms. Where the solitary structures are well separated from each other such as early in panel e in Fig. 11, the voltage again swings first negative and then positive.

2.7. E17 Observations

The E17 pass is a wake passage with a closest approach altitude of 3582 km on the anti-Jupiter facing hemisphere of Europa. As seen in Fig. 1, the geometry of the E17 flyby is very similar to both E11 and E15 except that E17 was approximately $2R_E$ south of Europa's equatorial plane throughout the pass. There were no recorded observations available from the E17 flyby of Europa; however, compressed realtime science observations were obtained which provide an overview of the plasma wave observations from this pass shown in Fig. 3c. ECH bands at $3f_{ce}/2$ and $5f_{ce}/2$

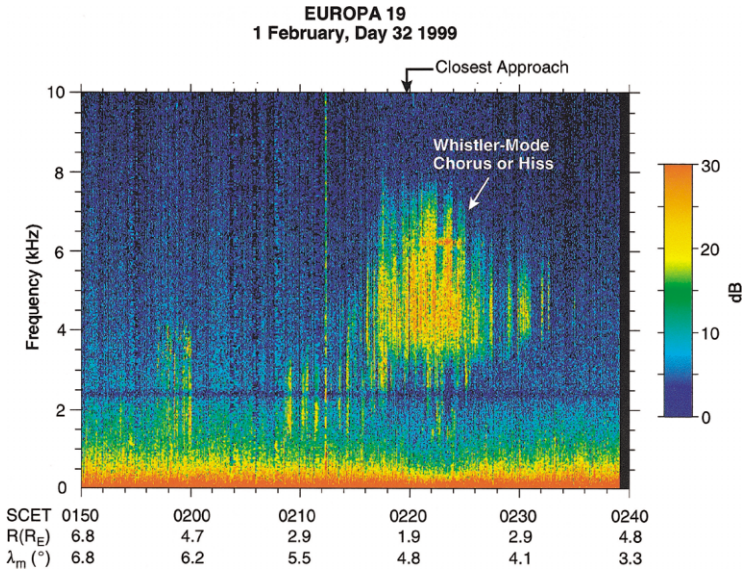

Fig. 12. Wideband spectrogram for the E19 flyby in the 10-kHz mode.

are seen early in this interval; however, these occur at the magnetic equator crossing, hence, are not thought to be associated with the Europa flyby. There is no obvious enhancement in the low-frequency whistler-mode band below 1 kHz. There are bursty emissions between about 0355 and 0405 SCET above 1 kHz but below f_{ce} and, at smaller amplitudes extending above f_{ce}. Some of these higher frequency emissions may extend as late as about 0425 SCET with a particular enhancement just above f_{ce}, suggesting that these may be $3f_{ce}/2$ emissions. The broadband bursty emissions precede the geometric wake by a few minutes, but extend for just less than the expected duration for the wake region. Note that these electrostatic waves are seen as in the other wake passages despite the large southward displacement of this flyby relative to Europa's equator (see the bottom panel of Fig. 1). There is evidence in the magnetic field spectrogram for weak, brief chorus emissions with a gap at one-half f_{ce} near the entrance to the geometric wake region. The upper hybrid band runs continuously through the plotted interval at $\sim$ 125 kHz, giving an electron density of just under 200 cm^{-3}. The density profile for this flyby is shown in Fig. 5. Interestingly, the enhancement in the f_{UH} band centered on 0445 SCET occurs well after both closest approach and the wake passage; it is apparently not associated with Europa.

2.8. E19 Observations

The E19 trajectory is shown in Fig. 1. This is an upstream pass similar in most respects to that of E6, but with a closest approach altitude of 1439 km, considerably higher than in E6. E19 also lies nearly $1R_E$ north of Europa's equatorial plane while E6 is about $0.5R_E$ south of the equator. The magnitude of the Jovicentric magnetic latitude of the two passes is similar, although E6 is 7.6° south whereas E19 is 5.6° north. Contrary to what is observed on E6, there is no clear enhancement in the broadband, low-frequency whistler-mode emissions observed in either the electric or magnetic sensors as seen in Fig. 3d. There is, however, a clear whistler-mode band at a few kHz centered at about 0222 SCET, well after the closest approach. The upper hybrid band is at a nearly constant frequency just above 100 kHz for the first half of the interval shown, but rises slightly just before closest approach. As seen in Fig. 5, the density is $\sim$ 100 cm^{-3} early and nearly 200 cm^{-3} after about 0215 SCET. There is no enhancement of this upper hybrid band.

Wideband observations in the 10-kHz mode shown in Fig. 12 resolve the lower-resolution observations given in Fig. 3d. The band of whistler-mode emissions centered near 0222 SCET is seen to have little spectral structure, suggesting whistler-mode hiss as opposed to chorus, however, the very narrowband emission at 6.3 kHz is unique among the Europa observations. Chorus emissions observed by Voyager and described by Coroniti et al. (1984) do show similar narrowband intensifications in the chorus spectrum. Bursty emissions occur at lower frequencies near 0200 and again near 0210 SCET. While these are in the whistler-mode frequency range, we cannot tell whether these are electrostatic or electromagnetic emissions.

2.9. E26 Observations

E26 is the first flyby of the second extension of the Galileo mission at Jupiter. The geometry of the flyby is shown in Fig. 1 and it is unique among the nine presented here. Because of the much lower perijove of this orbit, the trajectory in the coordinate system of Fig. 1 is nearly radial toward Jupiter. Furthermore, from a strictly geometric point of view,

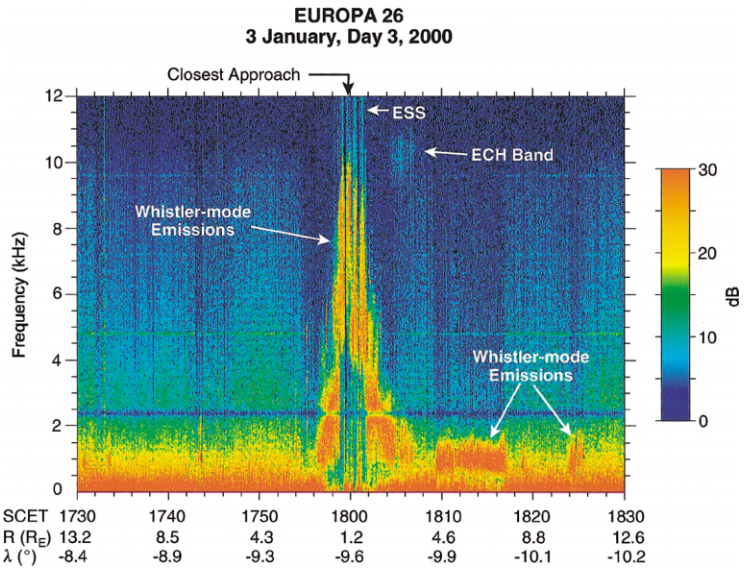

Fig. 13. Wideband spectrogram for the E26 flyby in the 10-kHz mode.

it represents a possible flux tube crossing as it crosses south of the disk of Europa near closest approach which occurs at 1759:43 SCET at an altitude of 198 km. The observations are summarized in Fig. 4. The most prominent wave activity of this flyby is centered near closest approach and is evidently whistler-mode in nature based on the magnetic component seen above 2.4 kHz in the upper panel and the fact that these emissions are at or below 10 kHz, hence, almost certainly below f_{ce}. There are, however, electrostatic emissions that extend well above 10 kHz to and above f_{UH} near closest approach. These appear to be related to emissions which extend down to 5 Hz in the electric field panel. Since there is no evidence of these lower frequency emissions in the bottom of the magnetic panel, it is possible these are electrostatic solitary structures. The upper hybrid band is intensified near closest approach and lower harmonic ECH bands are quite prominent after closest approach. The upper hybrid band is used to determine a density profile as provided in the bottom panel of Fig. 5. A strong band of whistler mode emission is seen centered near 1 kHz on the outbound portion of the flyby between about 1810 and 1818 SCET.

The E26 wideband observations obtained in the 10-kHz mode are presented in Fig. 13. The whistler-mode emissions exhibit an extraordinary Λ form in the frequency–time spectrogram with the peak frequency occurring very close to closest approach. However, superimposed on this Λ-shaped emission are broadband bursty structures similar to those associated with electrostatic solitary structures observed in the wake during other passes. The very intense whistler mode emissions clearly drive the gain of the AGC receiver to a low value and, consequently, the broadband emissions do not appear as intense as they might in the absence of the whistler mode waves. An examination of waveforms during this time period are suggestive of solitary structures, even though the intense whistler-mode waves make it difficult to clearly distinguish them. Interestingly, these broadband bursty emissions appear for a time period approximately the same as when the spacecraft is directly south of the disk of Europa. The similarity of these electrostatic solitary structures to those found in the wake is strongly suggestive of a connection between the wake region and the flux tube threading the moon.

Fig. 13 also shows the low-frequency whistler-mode band after closest approach and a second, shorter emission at about the same frequency centered near 1825 SCET.

3. Discussion and conclusions

The region within several R_E of Europa is the location of electrostatic electron–cyclotron harmonic and upper hybrid resonance emissions, whistler-mode emissions, and electrostatic solitary structures, sometimes referred to as broadband electrostatic noise. In this section we will briefly discuss the nature of these waves and why they might be associated with the magnetosphere–Europa interaction. We will also review the observations and try to compile a simple model which describes where these emissions are most likely to be found with respect to Europa.

3.1. Electrostatic solitary structures in the wake

Perhaps the most repeatable phenomenon in the wave spectrum near Europa is the existence of bursty, broadband electrostatic waves or electrostatic solitary structures in the geometric wake of the moon and its flux tube. We have shown examples of both bipolar and monopolar structures and events with characteristic time scales of 0.1 to a few ms. The last several years have seen a tremendous expansion of our understanding of such structures in the terrestrial

magnetosphere including an appreciation for their importance and the role they play in coupling various regions of the magnetosphere and even between the ionosphere and magnetosphere. Temerin et al. (1982) and Boström et al. (1988) have reported negatively charged structures in the terrestrial auroral zone. These have been identified as weak double layers or ion holes. Boström et al. estimated scale sizes between 5 and $50\lambda_D$ and speeds at the ion acoustic speed c_s. However, McFadden et al. (1999) suggest that the velocities reported by Boström et al. may be low because of instrumental considerations and Bounds et al. (1999) point out that the ion hole speeds are probably more comparable with ion beam speeds and, as a consequence, the ion holes are larger than the Boström et al. estimate. Other similar, but faster phenomena have been reported by Matsumoto et al. (1994) in the geomagnetic tail and more recently by Franz et al. (1998, 2000) and Ergun et al. (1998) in the auroral region. These studies have identified the faster electrostatic solitary structures as electron holes with length parallel to the magnetic field of about $2\lambda_D$ moving along the field line at a fraction of the electron thermal speed.

Galileo observes the electrostatic structures in Europa's wake with a single-dipole antenna which does not allow the measurement of vector components, nor does it allow the separation of spatial scale from speed, as can be done, for example, by the Polar wave instrument (Franz et al., 2000). Further, without being able to measure the direction of motion, Galileo cannot determine the charge of the structures to determine whether they are electron or ion holes. Galileo can only measure the time duration Δt of the events, which is related to the size L and speed v_{st} by

$$\Delta t = L/v_{st}. \quad (1)$$

While we cannot unambiguously identify these structures as either electron or ion holes, there are some considerations which may be relevant to the question. First, the electron holes appear to be much more ubiquitous in the terrestrial magnetosphere based on the Geotail and Polar observations. The ion holes, on the other hand, appear to be confined to auroral field lines near the acceleration region below a couple of Earth radii in altitude (S.R. Bounds, pers. commun., 2000). This might argue more for an electron hole interpretation for the structures seen in the wake of Europa. Second, the observed Δt shown herein is closer to those observed for electron holes and significantly smaller than those for ion holes at Earth.

Of course simply comparing the observed Δt with those of electron and ion holes at Earth ignores the plasma conditions in each case; it would be better if one could scale the expected sizes and velocities for electron and ion holes and compare these scaled ratios to the Δt's observed by Galileo. Franz et al. (2000) suggest that the size of electron holes parallel to the magnetic field do scale as about $2\lambda_D$. Using ion-hole velocities of a few hundred km s^{-1} (Bounds et al., 1999), we can use $50–500\lambda_D$ for the relevant scale size of ion holes, but it is not clear whether this is simply their observed size or that they actually scale to the Debye length. For the moment, however, we will assume that the size does scale in this manner. We will now investigate the Europa structures with such scaling in mind. Even this type of analysis is difficult, however, because of the lack of complete information on the plasmas in the wake region. Those that we have are the electron densities reported by Gurnett et al. (1998) and herein and the ion measurements from Paterson et al. (1999) who report on plasma observations during the E4 and E6 flybys. From the latter report, we take 2×10^6 K as typical the ion temperature. The density, taken from Fig. 5, ranges between about 60 and 125 cm^{-3} in the E4 wake.

We first make the hypothesis that the Europa structures are similar to the ion holes discussed by Boström et al. (1988). We use $L = a\lambda_D$ and $v_{st} = 10c_s$ as empirical determinations of the ion-hole size and speed. The factor of 10 is due to the suggested underestimate of the ion velocity of the Viking results and the suggestion by Bounds et al. (1999) that the ion-hole speeds are closer to the ion-beam speed. We substitute for λ_D and c_s using

$$\lambda_D = 743\sqrt{\frac{T_e}{n_e}}$$

and

$$c_s = 9.8 \times 10^5 \left(\frac{\gamma Z T_e}{\mu}\right)^{1/2},$$

where λ_D is in cm, c_s is in cm s^{-1}, T_e is in eV, γ is the adiabatic index, and Z/μ is the charge to mass of the ions. Eq. (1) then becomes

$$\Delta t = \frac{743a}{2.8 \times 10^6 \sqrt{n_e}}$$

where we have taken γ of order 1 and $\mu/Z = 12$ based on Paterson et al. (1999). Notice that the electron temperature factors out and Δt is only a function of the electron density and the factor a. Now, we use an intermediate value of 80 cm^{-3} for n_e, 1 ms for Δt and solve for a. The result is 34 which is somewhat smaller than the range of 50–500. If we take $T_e = T_i$ for lack of any better information, then $v_{st} \sim 370$ km s^{-1} and $L \sim 370$ m. This speed is in the range given for ion holes given, for example, by Bounds et al. (1999), but the implied size is smaller than those at Earth by a factor of 5 or so. In the case where $\Delta t = 0.1$ ms this calculation gives even smaller values of L.

We can now try the alternate hypothesis that the structures in the wake of Europa are electron holes which have a parallel length of $L \sim 2\lambda_D$ and move along the field with at a fraction b of the electron thermal speed $v_{st} = 4.2 \times 10^7 b\sqrt{T_e}$. As in the ion-hole argument above, the electron temperature drops out of the equation for Δt:

$$\Delta t = \frac{2 \cdot 743}{4.2 \times 10^7 b \sqrt{n_e}}.$$

Again, taking $\Delta t = 1$ ms and $n_e = 80$ cm^{-3} we can solve for b which is 0.004 for the parameters selected. Given that the fraction b in the terrestrial case is of order 1, it would

appear that the electron-hole hypothesis does not fit the observed Δt very well. Reported speeds for the electron holes at Earth are of order 1000 km s^{-1}, significantly greater than the 22 km s^{-1} implied by the above calculation.

In summary, while we are confident that the electrostatic solitary structures are analogous to those observed at Earth we are not confident in being able to identify the electrostatic solitary structures as specifically electron or ion holes.

Ergun et al. (1998) suggest that the electron holes studied at Earth play a significant role in the auroral acceleration region, possibly providing the anomalous resistivity required to support field-aligned potentials. Ion holes also play an important role in terrestrial auroral physics by interacting nonlinearly with ion beams (Bounds et al., 1999). This nonlinear interaction likely includes acceleration and heating of particles.

3.2. Whistler-mode emissions

Whistler-mode emissions are generated by anisotropies in the electron distribution function such as a loss-cone or an anisotropy between the parallel and perpendicular temperatures. The characteristic energy E_c of electrons for the whistler mode is given by

$$E_c = \frac{B^2}{2\mu_0 n_e},$$

using typical parameters for the Europa environment of $f_{pe}=$ 100 kHz ($n_e = 124$ cm^{-3}) and $f_{ce} = 12$ kHz ($B = 429$ nT), $E_c \approx 3.7$ keV. The resonant energy E_r for frequency f, then, is

$$E_r \cong E_c \frac{f_{ce}}{f}\left(1 - \frac{f}{f_{ce}}\right)^3. \quad (2)$$

Hence, for the band-limited emissions near 3 kHz we can use Eq. (2) and compute the resonant energy which is of the order of 6 keV. For the lower frequency hiss (e.g. observed during E4 and E6) at 300 Hz the resonant energy is of order 140 keV.

There are three ways in which Europa could enhance the generation of whistler mode emissions. First, since the characteristic energy of electrons resonant with the whistler mode is $B^2/2\mu_0 n_e$, if the magnetic field intensity is depressed by either an intrinsic or induced magnetic field effect as seems to be the case for E4, E11, and E15 (Kivelson et al., 1999; M.G. Kivelson, pers. commun., 1999), then the characteristic energy is decreased and, hence, larger fluxes of electrons would be at the resonant energy. Likewise, if the electron density is enhanced, the resonant energy is also decreased. There is some evidence for enhanced electron densities near Europa as presented herein, but this is not a strong effect and is quite variable. The influence of the Io torus all but dominates the plasma density at Europa's orbit. However, if Europa is a sink for electrons at some pitch angles or if newly created plasma is a result of the magnetosphere–Europa interaction as is suggested by Paterson et al. (1999), then it is possible that enhanced anisotropy in the electron distribution function could be responsible for the Europa-related whistler-mode emissions. It is curious that the whistler modes are not observed in the wake region, where it would be natural to find the scavenged Europa plasma. Energetic charged particle observations near Europa (Paranicas et al., 2000) show pitch angle dependent decrease in count rates of particles in many channels including electrons both in the wake and upstream, consistent with absorptions by the moon. Decreases in the electron count rate during the E4 pass correspond in time to the intense whistler-mode hiss between 0650 to 0655 SCET. Here, the electron energies shown by Paranicas et al. to exhibit pitch-angle dependent decreases are in the range of 42–65 keV, well within the range of resonant energies calculated above.

3.3. Electron–cyclotron harmonics and upper hybrid band enhancements

The region of the Jovian magnetosphere at and inside the orbit of Europa is often characterized by a relatively weak band of emission at the upper hybrid resonance frequency. At the magnetic equator, this band is almost always enhanced. The equatorial emissions are a special case of the electron–cyclotron harmonic emissions (cf Kurth et al., 1979; Ashour-Abdalla and Kennel, 1978) which are instabilities caused by positive slopes in the perpendicular electron distribution function. Growth at the upper hybrid band is supported by a large ratio of cold to hot electrons n_c/n_h (Hubbard and Birmingham, 1978; Ashour-Abdalla and Kennel, 1978) and the intensification appears to be further supported by propagation properties near the magnetic equator which keep the waves in the region of maximum growth (Barbosa, 1980; Engle and Kennel, 1984). The weaker emissions off the magnetic equator are more likely thermal emissions such as the terrestrial emissions discussed by Sentman (1982). We have attempted to distinguish Europa-related enhancements in the upper hybrid bands from the ambient equatorial enhancements by identifying only those well off the magnetic equator as being associated with Europa. Drawing from our knowledge of the equatorial enhancements, however, we can suppose that the Europa-related upper hybrid enhancements could be due to one or more possible conditions imposed by Europa. First, if Europa is a source of plasma, it is likely that this new plasma is cold relative to the magnetospheric plasma and the condition of $n_c/n_h > 1$ is more likely. Second, electron losses near Europa or newly picked-up electrons may cause accentuated loss cones or other anisotropies which could drive the electron–cyclotron harmonic instability. Finally, the distortion of the magnetic field in the vicinity of Europa may affect the propagation of the electrostatic waves in such a way as to increase the

convective growth rate of the waves. If the distortion is a depression in the field strength, the situation is similar to the magnetic equator in that the equator is a minimum B region.

It is less clear how the low-harmonic electron–cyclotron bands seen well upstream of Europa arise. In general, they are driven by electron distributions similar to those responsible for the upper hybrid emissions, but with a relatively smaller population of cold electrons. It may be possible that anisotropies associated with Europa can be found a few R_E upstream of the moon, or that these anisotropies are sufficiently durable to persist from a previous passage of the plasma past the moon, in the sense of an extended plasma plume. At the larger distances upstream from Europa, though, it is less likely that there would be a substantial population of cold electrons originating from the moon.

3.4. A model for the plasma-wave regimes near Europa

A brief glance at Figs. 2–4 shows little apparent similarity in the plasma-wave spectra from one flyby to the next. In fact, it is the motivation of this paper to attempt to understand these apparently disparate observations. Table 1 provides information on a number of geometric characteristics of the flybys which may play a role in organizing the observations. Also, Fig. 1 allows us to approach the problem by comparing observations from similar trajectories. For example, E11, E15, and E17 all have very similar geometries and the wave spectra show some general similarities. Perhaps the most obvious is the presence of broadband electrostatic noise (or electrostatic solitary structures) in the vicinity of the wake. This characteristic is also shared by the E4 wake passage. In each of these passes the bursty electrostatic signatures are seen over an interval of time similar to but somewhat shorter than the extent of the geometric wake. There is often a mismatch of a few minutes between the onset of the signature and the entry into the wake. We suggest that such timing inconsistencies are simply explained by rotations in the magnetospheric flow past Europa from the nominal corotation direction by the addition of a relatively small radial component. The broadband electrostatic noise is generally less pronounced later in the wake flyby. Based on the geometry, the latter portion of the wake passage is always at larger downstream distances, hence, the decrease in electrostatic noise intensity could suggest a dissipation in turbulence in the more distant wake. The E26 observations of electrostatic solitary structures in the flux tube and the decreasing intensity of these in the more distant wake suggest that the beams and/or currents which likely are related to these structures are initiated in the flux tube and then continue for some time after the magnetic field has convected downstream of the moon.

The broadband enhancement in emissions below f_{ce} is also a common feature in the wake, however for most passes we cannot make a clear assessment of the nature of these waves because of the lack of reliable magnetic component measurements. In E4, however, this enhancement is clearly more consistent with electrostatic waves than the whistler-mode. It is likely, however, that there is an admixture of both electrostatic and electromagnetic modes in this region. But such whistler-mode waves are a normal feature of the ambient Io plasma torus (Gurnett et al., 1996), so they may have nothing to do with the presence of Europa.

Another component common to the E11 and E15 passes is the band-limited whistler-mode emission near a few kHz occurring prior to entry into the wake. It is likely, however, that these emissions are ambient magnetospheric emissions for E15 because of this encounter's proximity to the magnetic equator. The E19 flyby, an upstream pass, also shows this feature. This band of emission, when present, is usually found within $\sim 2R_E$ of Europa.

There are two other sets of similar flyby geometries to examine. The first is the E6–E19 pair, both of which are upstream passes with closest approach on the Jupiter-facing hemisphere of Europa. These two passes are at similar magnetic latitudes with respect to Jupiter, albeit in opposite hemispheres. The wave spectra for these two flybys have surprisingly little in common despite the similar trajectories. E6 is dominated by broadband whistler-mode emission from $\sim$10 Hz to near the expected electron–cyclotron frequency of $\simeq$12 kHz. On E19, the primary whistler-mode emission is clearly band limited and above about 2 kHz. We do not understand the nature of this difference. It is likely the generation mechanism is similar, but perhaps the band limited waves exist because of a lack of anisotropic electrons at higher energies. Another difference between these two sets of observations is the lack of enhancement of the upper hybrid band in the E19 data set. Since this enhancement often occurs near closest approach, it is possible that the considerable difference in closest approach altitudes (586 km for E 6 versus 1439 km for E19) plays a role in this particular difference. The upper hybrid instability requires a large population of cold electrons (Ashour-Abdalla and Kennel, 1978) and if there were a cold plasma source at Europa, it would be more influential closer to the moon.

The final pair of similar flyby trajectories are E12 and E14, both of which are upstream passes with closest approach on the anti-Jupiter hemisphere. These two sets of observations are quite different, also. There are virtually no variations in the plasma wave spectrum at all during the E14 flyby, strongly suggesting no strong interaction with Europa. The only exception would be the very weak ECH band well upstream of the moon seen near 1311 SCET in Fig. 3a. There is no evidence of enhanced whistler-mode activity, either broadband or band limited and only a very weak upper hybrid band during the E14 pass. Since the E12 flyby occurs near the magnetic equator, it is possible that the band-limited whistler-mode noise observed during that flyby is not associated with Europa. In this case, there is little difference between the Europa-related signatures for these two flybys. If the E12 whistler-mode emission is due to Europa, one could

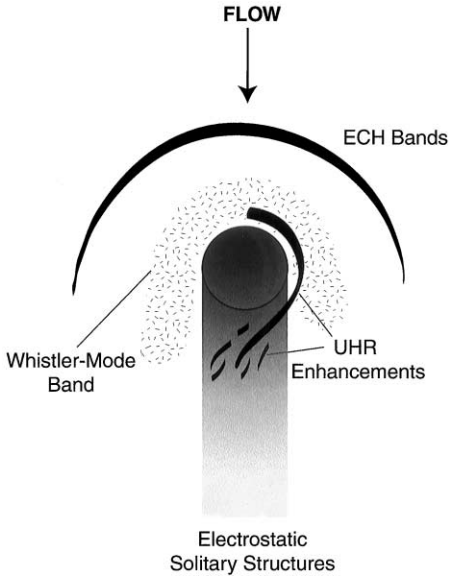

Fig. 14. A schematic showing the general locations where various plasma wave features are observed in the vicinity of Europa based on the observations presented herein.

conclude that the large flyby altitude difference between the two trajectories is primarily responsible for the difference in the occurrence of these emissions.

We have attempted to describe the occurrence of the various plasma wave signatures observed near Europa with the use of a schematic model illustrated in Fig. 14. Here, we show Europa with the nominal corotational flow moving from top to bottom in a coordinate system like that shown in the top panel of Fig. 1. This illustration is meant to help us and the reader assimilate the numerous and often disparate observations presented herein. However, it is important to not read too much into the details of this model. While it is drawn more-or-less to scale, limitations in the volume mapped by Galileo and time variations suggest that distances not to be taken too seriously. Also, the actual regions of occurrence are almost certainly more irregular than those shown and temporal variations also will affect where and even whether a particular emission is present or not. Nevertheless, there is some value in describing the observations in the context of this schematic. ECH bands, typically near $3f_{ce}/2$, if observed at all, are seen at rather large distances upstream and on the flanks of the interaction region. The whistler-mode emissions, whether band limited or broadband, occur quite close to Europa and generally outside of the wake region. The enhancement in the upper hybrid band (and sometimes lower harmonic ECH bands) is most obvious near closest approach and sporadically in the wake. The wake and flux tube region is consistently the site of broadband electrostatic noise (electrostatic solitary structures) with dramatic differences on time scales of a second or less.

We have suggested that the modified magnetic field near Europa, enhancements in the electron density due to the plasma source at the moon, and anisotropies in the electron distribution function due to losses and sources at Europa may all contribute to the whistler-mode and upper hybrid resonance emissions near the moon. The electrostatic solitary structures are likely associated with beams or currents flowing in the flux tube and wake as a result of the Europa–magnetospheric interaction. None of these conclusions rest on solid, quantitative footings at this time, but further studies primarily addressing the suprathermal electron distribution functions near Europa should help to address these shortcomings.

Liu et al. (2000) have recently produced a two-fluid MHD model of the Europa–magnetosphere interaction which reproduces measurements of the bulk plasma parameters reasonably well for the E4 flyby. This model shows that the primary perturbations associated with the interaction lie within about $1R_E$ on the upstream side of Europa with significantly longer scale influence on the flanks and especially downstream of Europa. Herein we report effects which apparently are associated with the interaction at distances of 2 to 3 times further, even in the upstream direction. We do not consider this a major disagreement, however, since the MHD model would not be expected to produce the instabilities discussed here, which are based on higher order moments of the plasma distribution function. Furthermore, the instabilities may be affected by rather small fractions of the plasma distribution, which may be found at distances significantly greater than the obvious first-order effects shown by Liu et al. Both of our models of the plasma wave environment as in Fig. 14 and Liu et al.'s model show reasonable symmetry about the axis parallel to the flow direction and significant effects in the wake region, so there is general agreement to the extent one might expect from a MHD model.

Acknowledgements

The research at the University of Iowa is supported by the National Aeronautics and Space Administration through Contract 958779 with the Jet Propulsion Laboratory. We are grateful to M.G. Kivelson and the Galileo Magnetometer team for making magnetic field intensities available to us for use in determining electron–cyclotron frequencies.

References

Ashour-Abdalla, M., Kennel, C.F., 1978. Multi-harmonic electron cyclotron instabilities. Geophys. Res. Lett. 5, 711–714.

Barbosa, D.D., 1980. On the convective properties of magnetospheric Bernstein waves. J. Geophys. Res. 85, 2341–2345.

Barbosa, D.D., Scarf, F.L., Kurth, W.S., Gurnett, D.A., 1981. Broadband electrostatic noise and field-aligned currents in Jupiter's middle magnetosphere. J. Geophys. Res. 86, 8357–8369.

Boström, R., Gustafsson, G., Holback, B., Holmgren, G., Koskinen, H., Kintner, P., 1988. Characteristics of solitary waves and weak double layers in the magnetospheric plasma. Phys. Rev. Lett. 61, 82–85.

Bounds, S.R., Pfaff, R.F., Knowlton, S.F., Mozer, F.S., Temerin, M.A., Kletzing, C.A., 1999. Solitary potential structures associated with

ion and electron beams near $1R_E$ altitude. J. Geophys. Res. 104, 28,709–28,717.

Coroniti, F.V., Scarf, F.L., Kennel, C.F., Kurth, W.S., 1984. Analysis of chorus emissions at Jupiter. J. Geophys. Res. 89, 3801–3820.

Engle, J., Kennel, C.F., 1984. Effect of parallel refraction of magnetospheric upper hybrid waves. Geophys. Res. Lett. 11, 865–868.

Ergun, R.E., Carlson, C.W., McFadden, J.P., Mozer, F.S., Delory, G.T., Peria, W., Chaston, C.C., Temerin, M., Roth, I., Muschietti, L., Elphic, R., Strangeway, R., Pfaff, R., Cattell, C.A., Klumpar, D., Shelley, E., Peterson, W., Moebius, E., Kistler, L., 1998. FAST satellite observations of large-amplitude solitary structures. Geophys. Res. Lett. 25, 2041–2044.

Franz, J.R., Kintner, P.M., Pickett, J.S., 1998. POLAR observations of coherent electric field structures. Geophys. Res. Lett. 25, 1277–1280.

Franz, J.R., Kintner, P.M., Seyler, C.E., Pickett, J.S., Scudder, J.D., 2000. Properties of coherent electric field structures observed by Polar. J. Geophys. Res. 27, 169–172.

Gurnett, D.A., Frank, L.A., 1977. A region of intense plasma wave turbulence on auroral field lines. J. Geophys. Res. 82, 1031–1050.

Gurnett, D.A., Frank, L.A., Lepping, R.P., 1976. Plasma waves in the distant magnetotail. J. Geophys. Res. 81, 6059–6071.

Gurnett, D.A., Kurth, W.S., Shaw, R.R., Roux, A., Gendrin, R., Kennel, C.F., Scarf, F.L., Shawhan, S.D., 1992. The Galileo plasma wave investigation. Space Sci. Rev. 60, 341–355.

Gurnett, D.A., Kurth, W.S., Roux, A., Bolton, S.J., Kennel, C.F., 1996. Galileo plasma wave observations in the Io plasma torus and near Io. Science 274, 391–392.

Gurnett, D.A., Kurth, W.S., Roux, A., Bolton, S.J., Thomsen, E.A., Groene, J.B., 1998. Galileo plasma wave observations near Europa. Geophys. Res. Lett. 25, 237–240.

Hubbard, R.F., Birmingham, T.J., 1978. Electrostatic emissions between electron gyroharmonics in the outer magnetosphere. J. Geophys. Res. 83, 4837–4850.

Kivelson, M.G., Khurana, K.K., Means, J.D., Russell, C.T., Snare, R.C., 1992. The Galileo magnetic field investigation. Space Sci. Rev. 60, 357–383.

Kivelson, M.G., Khurana, K.K., Joy, S., Russell, C.T., Walker, R.J., Polanskey, C., 1997. Europa's magnetic signature: Report from Galileo s first pass on December 19, 1996. Science 276, 1239–1241.

Kivelson, M.G., Khurana, K.K., Stevenson, D.J., Bennett, L., Joy, S., Russell, C.T., Walker, R.J., Zimmer, C., Polanskey, C., 1999. Europa and Callisto: Induced or intrinsic fields in a periodically varying plasma environment. J. Geophys. Res. 104, 4609–4625.

Kurth, W.S., Craven, J.D., Frank, L.A., Gurnett, D.A., 1979. Intense electrostatic waves near the upper hybrid resonance frequency. J. Geophys. Res. 84, 4145–4164.

Kurth, W.S., Barbosa, D.D., Gurnett, D.A., Scarf, F.L., 1980. Electrostatic waves in the Jovian magnetosphere. Geophys. Res. Lett. 7, 57–60.

Kurth, W.S., Bolton, S.J., Gurnett, D.A., Levin, S., 1997. A determination of the source of Jovian hectometric radiation via occultation by Ganymede. Geophys. Res. Lett. 24, 1171–1174.

Liu, Y, Nagy, A.F., Kabin, K., Combi, M.R., DeZeeuw, D.L., Gombosi, T.I., Powell, K.G., 2000. Two-species, 3D, MHD simulation of Europa's interaction with Jupiter's magnetosphere. Geophys. Res. Lett. 27, 1791–1794.

Matsumoto, H., Kojima, H., Miyatake, T., Omura, Y., Okada, M., Nagano, I., Tsutsui, M., 1994. Electrostatic solitary waves (ESW) in the magnetotail: BEN wave forms observed by GEOTAIL. Geophys. Res. Lett. 21, 2915–2918.

McFadden, J.P., Carlson, C.W., Ergun, R.E., 1999. Microstructure of auroral acceleration region as observed by FAST. J. Geophys, Res. 104, 14,453–14,480.

Paranicas, C., McEntire, R.W., Cheng, A.F., Lagg, A., Williams, D.J., 2000. Energetic charged particles near Europa. J. Geophys. Res. 105, 16,005–16,015.

Paterson, W.R., Frank, L.A., Ackerson, K.L., 1999. Galileo plasma observations at Europa: Bulk parameters. J. Geophys. Res. 104, 22,779–22,791.

Sentman, D.D., 1982. Thermal fluctuations and the diffuse electrostatic emissions. J. Geophys. Res. 87, 1455–1472.

Temerin, M., Cerny, K., Lotko, W., Mozer, F.S., 1982. Observations of double layers and solitary waves in the auroral plasma. Phys. Rev. Lett. 48, 1175–1179.